Anisotropic reverse-time migration for tilted TI media

Xiang Du, John C. Bancroft, and Larry R. Lines

ABSTRACT

Seismic anisotropy in dipping shales results in imaging and positioning problems for underlying structures. We develop an anisotropic reverse-time depth migration approach for P-wave and SV-wave seismic data in transversely isotropic (TI) media with a tilted axis of symmetry normal to bedding. Based on an accurate phase velocity formula and dispersion relationships for weak anisotropy, we derive the wave equation for P-wave and SV-wave propagation in tilted transversely isotropic (TTI) media. The accuracy of the P-wave equation and the SV-wave equation is analyzed and compared with other acoustic wave equations for TTI media. Using this analysis and the pseudo-spectral method, we apply reverse-time migration to numerical and physical-model data. According to the comparison between the isotropic and anisotropic migration results, the anisotropic reverse-time depth migration offers significant improvements in positioning and reflector continuity over those obtained using isotropic algorithms.

INTRODUCTION

Much hydrocarbon resource exploration and development involves classic dipping anisotropic sequences, and thick anisotropic sequences of dipping sandstones and shales often overlie the reservoir in fold and thrust belts, such as in the Canadian Foothills (Isaac and Lawton, 1999). In these cases, during data processing – particularly depth migration, with either an isotropic migration algorithm or a VTI assumption – there will be imaging problems and mispositioning errors. Anisotropic depth migration is required to correctly locate images when TTI strata are present. Alkhalifah (1995) proposed Gaussian beam depth migration for VTI media. Vestrum et al. (1999) adopted a ray-tracing algorithm to image structures below dipping TI media. Several methods have been proposed based on the operator used for wavefield extrapolation in laterally varying VTI media. Ferguson and Margrave (1999) addressed nonstationary phase-shift for TI media. Zhang et al. (2001) proposed short spatial convolution operators to extrapolate the wavefields recursively in space-frequency domain for both qP and qSV-waves in tilted TI media. Baumstein and Andersonet (2003) combined the phase-shift and explicit correction operators to solve the cost problem by using a shorter explicit correction operator. As a wave equation technique using a two-way hyperbolic wave equation, reverse-time migration (McMechan, 1983; Wu et al., 1996; Yoon et al., 2003) can handle not only multi-arrivals but also steep dips and overturned reflections. It propagates the measured wavefield backward in time using a hyperbolic wave equation and does not suffer from dip limitation of one-way downward continuation algorithms. Although numerical computation of the wave equation is expensive, rapid development of computer hardware enables reverse-time migration to be widely used in production image problems (Yoon et al., 2003). In this paper, we present an anisotropic reverse-time migration for tilted transversely isotropic media. We derive the P-wave equation and SV-wave equation for TTI media from Thomsen's (1986) phase velocity formula. We also analyze the accuracy of these equations. Examples of numerical and physical models are shown to demonstrate the effectiveness of reverse-time migration in dipping media.

THEORY

Simplified P and SV wave equation for TTI media

To simulate acoustic-wave propagation in a medium with a vertical axis of symmetry (VTI), Alkhalifah (2000) proposed an acoustic wave equation by simply setting the shear wave velocity to zero. He showed that the new acoustic VTI wave equation yields a kinematically good approximation of P-wave propagation as compared to the full elastic solution in VTI media. Zhang et al. (2003) extended the acoustic wave equation for VTI media to one for TTI media. In fact, contrary to the conventional wisdom that setting Vs_0 equal to 0 eliminates shear waves, the acoustic wave equation introduces diamond-shape artifacts, which means that it does not eliminate the shear wave phase velocity in other directions. Klie and Toro (2001) used a weak anisotropy approximation to successfully suppress these "artifacts". Grechka et al. (2004) gave a detailed discussion about the shear waves in acoustic anisotropic media. Alkhalifah (2000) proposed placing a thin isotropic layer between the source and the first anisotropic medium, but this imposes limitations to his formulation not only for modeling anisotropic cases, but also for possible extensions to other seismic processing and imaging stages. Strong shear waves will contaminate P-wave data produced by any full waveform modeling code (Grechka et al., 2004). Moreover, imaging techniques such as reverse-time migration will have artifacts due to the shear waves. To implement the P and SV wave reverse-time migration in TTI media, we need to get the individual P wave and SV wave equations. We start with the VTI phase-velocity equation (Tsvankin, 1996) written as

$$\frac{V^2(\theta)}{V_{p0}^2} = 1+\varepsilon\sin^2\theta - \frac{f}{2} \pm \frac{f}{2}\sqrt{(1+\frac{2\varepsilon\sin^2\theta}{f})^2 - \frac{2(\varepsilon-\delta)\sin^2 2\theta}{f}}. \quad (1)$$

When we rotate the symmetry axis from vertical to a tilt angle ϕ, the phase velocity in the direction measured from the vertical direction is:

$$\frac{V^2(\theta,\phi)}{V_{p0}^2} = 1+\varepsilon\sin^2(\theta-\phi) - \frac{f}{2} \pm \frac{f}{2}\sqrt{(1+\frac{2\varepsilon\sin^2(\theta-\phi)}{f})^2 - \frac{2(\varepsilon-\delta)\sin^2 2(\theta-\phi)}{f}}, \quad (2)$$

where V_{p0} is vertical velocity and $f = 1-\frac{V_{s0}^2}{V_{p0}^2}$. V_{p0} and V_{s0} are qP-wave and qS-wave velocity respectively. ε and δ are Thomsen parameters (Thomsen, 1986), which are defined as:

$$\varepsilon = \frac{c_{11} - c_{33}}{2c_{33}}\ ;\ \delta = \frac{(c_{13} + c_{44})^2 - (c_{13} - c_{44})^2}{2c_{33}(c_{13} - c_{44})}\ ; \tag{3}$$

where c_{ij} are elastic moduli. Noting that anisotropic reverse-time migration is expensive and weak anisotropy is a reasonable assumption in many real systems (Thomsen, 1986), we make the assumption of weak anisotropy, which saves computational effort while retaining computational accuracy. This allows us to transform the phase-velocity expression of Equation (2). Expanding the radical in a Taylor series and dropping quadratic terms in the anisotropy parameters ε and δ, we can obtain the P-wave and SV-wave phase velocity formula as:

$$\frac{V_p^2(\theta)}{V_{p0}^2} = 1 + 2\delta\sin^2\theta\cos^2\theta + 2\varepsilon\sin^4\theta\,, \tag{4}$$

$$\frac{V_s^2(\theta)}{V_{p0}^2} = 1 - f + 2(\varepsilon - \delta)\sin^2\theta\cos^2\theta\,. \tag{5}$$

To obtain Alkhalifah's acoustic wave equation for anisotropic VTI media, Alkhalifah (2000) simply set $V_{s0} = 0$, which makes $f = 1$. Then from Equation (2), the acoustic wave equation can be written as

$$\frac{V_p^2(\theta)}{V_{p0}^2} = \frac{1}{2} + \varepsilon\sin^2\theta \pm \frac{1}{2}\sqrt{(1 + 2\varepsilon\sin^2\theta)^2 - 2(\varepsilon - \delta)\sin^2 2\theta}\,. \tag{6}$$

By rotating the symmetry axis from vertical to a tilt angle ϕ, we can get the phase velocity for P and SV waves in the direction measured from the vertical direction. The P and SV wave phase velocity formulas are shown as follows:

$$\frac{V_p^2(\theta,\phi)}{V_{p0}^2} = 1 + 2\delta\sin^2(\theta - \phi)\cos^2(\theta - \phi) + 2\varepsilon\sin^4(\theta - \phi)\,, \tag{7}$$

$$\frac{V_s^2(\theta)}{V_{p0}^2} = 1 - f + 2(\varepsilon - \delta)\sin^2(\theta - \phi)\cos^2(\theta - \phi)\,. \tag{8}$$

Using a similar approach, we can write the Alkhalifah acoustic wave equation for tilt angle ϕ as

$$\frac{V_p^2(\theta,\phi)}{V_{p0}^2} = \frac{1}{2} + \varepsilon\sin^2(\theta - \phi) \pm \frac{1}{2}\sqrt{(1 + 2\varepsilon\sin^2(\theta - \phi))^2 - 2(\varepsilon - \delta)\sin^2 2(\theta - \phi)}\,. \tag{9}$$

If we try to keep higher accuracy for weak anisotropy, we also can expand the radical in Equation (2) in a Taylor series and retain the quadratic terms in ε and δ. After tedious derivation, we obtain

$$\frac{V_p^2(\theta)}{V_{p0}^2} = 1 + 2\delta\sin^2\theta\cos^2\theta + 2\varepsilon\sin^4\theta + \frac{4}{f}(\varepsilon-\delta)(\varepsilon\sin^2\theta + \delta\cos^2\theta)\sin^4\theta\cos^2\theta, \quad (10)$$

$$\frac{V_s^2(\theta)}{V_{p0}^2} = 1 - f + 2(\varepsilon-\delta)\sin^2\theta\cos^2\theta - \frac{4}{f}(\varepsilon-\delta)(\varepsilon\sin^2\theta + \delta\cos^2\theta)\sin^4\theta\cos^2\theta. \quad (11)$$

For plane waves travel in the vertical (x, z)-plane, the phase angle is given by

$$\sin\theta = \frac{v(\theta,\phi)k_x}{\omega}, \quad \cos\theta = \frac{v(\theta,\phi)k_z}{\omega}. \quad (12)$$

When we multiply equations (7) and (8) with the wavefield in the Fourier domain $U(k_x, k_z, t)$, and apply an inverse Fourier transform with ($k_x \to -i\frac{\partial}{\partial x}, k_z \to -i\frac{\partial}{\partial z}, \omega \to i\frac{\partial}{\partial t}$), we can obtain P-wave and SV-wave equations in the time-wavenumber domain for TTI media. The P-wave equation for tilted transversely isotropic media is

$$\begin{aligned}\frac{\partial^2 U_p(k_x,k_z,t)}{\partial t^2} = -V_{p0}^2[&k_x^2 + k_z^2 + (2\delta\sin^2\phi\cos^2\phi + 2\varepsilon\cos^4\phi)\frac{k_x^4}{k_x^2+k_z^2} \\ &+ (2\delta\sin^2\phi\cos^2\phi + 2\varepsilon\sin^4\phi)\frac{k_x^4}{k_x^2+k_z^2} \\ &+ (-\delta\sin^2 2\phi + 3\varepsilon\sin^2 2\phi + 2\delta\cos^2\phi)\frac{k_x^2k_z^2}{k_x^2+k_z^2} \\ &+ (\delta\sin 4\phi - 4\varepsilon\sin 2\phi\cos^2\phi)\frac{k_x^3k_z}{k_x^2+k_z^2} \\ &+ (-\delta\sin 4\phi - 4\varepsilon\sin 2\phi\sin^2\phi)\frac{k_z^3k_x}{k_x^2+k_z^2})]U_p(k_x,k_z,t)\end{aligned} \quad . \quad (13)$$

The SV-wave equation for tilted transversely isotropic media is

$$\begin{aligned}\frac{\partial^2 U_s(k_x,k_z,t)}{\partial t^2} = -V_{s0}^2[&k_x^2 + k_z^2 + \frac{\sigma}{2}(2\sin^2 2\phi\frac{k_x^4 + k_z^4 - 2k_x^2k_z^2}{k_x^2+k_z^2} + 4\cos^2\phi)\frac{k_x^2k_z^2}{k_x^2+k_z^2} \\ &+ 4\varepsilon\sin 2\phi\cos^2\phi)\frac{k_xk_z(k_x^2-k_z^2)}{k_x^2+k_z^2}]U_s(k_x,k_z,t)\end{aligned} \quad . \quad (14)$$

$$\sigma = (\frac{V_{p0}}{V_{s0}})^2(\varepsilon-\delta)$$

In anisotropic seismic modeling and migration, we can use equations (13) and (14) to obtain separate P and SV wavefields. Daley and Lines (2004) advocate the formalism for Equation (14), which use (σ, ε) as parameters rather than (δ, ε).

Discussion of the Simplified P and SV wave equation for TTI media

To analyze the accuracy of the wave equations, the relationship between phase velocity and phase angle is discussed. We compare the difference among the weak anisotropy formula, the Alkhalifah acoustic wave formula and the exact P-wave phase

velocity formula for TTI media. Figure 1 shows the P-wave phase velocity and phase angle curves with 0, 30, 60, and 90 degree dipping angles and $\varepsilon = 0.25$, $\delta = 0.1$. There is only a slight difference among them for weakly anisotropic media. Figure 2 corresponds to the SV case comparison between phase velocities for weak anisotropy with linear approximation, moderate anisotropy with quadratic approximation, and the exact SV-wave solution for TTI media. There is some difference for the linear solution; however, if Equation (8) is modified by retaining the quadratic terms in ε and δ from the exact SV phase velocity formula, the accuracy is greatly improved. This of course requires increasing the computational cost.

We also display the relationship between P-wave and SV-wave phase velocities of Figure 1 and 2 in polar coordinates as shown in Figure 3. This reflects the wavefield snapshot to some extent, where the red curve denotes velocity based on the simplified Thomsen formula, whereas the blue curve is the exact phase velocity. The upper graphs show P-wave phase velocity curves with 0, 30, 60, and 90 degree dipping angles. The lower graphs correspond to the SV-wave phase velocity curves with same dipping angles. In the case of P-waves, there is hardly any difference between the simplified and exact formulas. Some differences exist in the SV wave curves, but the shapes are fairly consistent.

In Figure 3, we can observe a maximum difference the true and the liner approximation phase velocities that we refer to as the maximum velocity difference. The parameters ε and δ were varying from 0 to 0.25 with an increment of 0.01 to estimate a distribution of absolute maximum velocity difference. The absolute maximum velocity difference is plotted as a histogram in Figure 4 that shows the absolute maximum velocity difference values are mainly distributed within a 20m/s range that implies minimal variance. Consequently the simplified formula can be accurately used in seismic modeling and processing in the tilted transversely isotropic media.

Numerical solution method for P and SV wave equations for TTI media

The P-wave and SV-wave equations (Equation 13 and 14) can also be written in the time-space domain. However, space and time are coupled in the terms $\partial^4 u / \partial x^2 \partial t^2$ and $\partial^4 u / \partial z^2 \partial t^2$, and these cause computational difficulty in difference schemes, whereas the equations are easily solved in the time-wavenumber domain. Therefore the pseudospectral method is selected in reverse-time migration (RTM). The pseudospectral method (Fornberg, 1987) is a higher accuracy method that needs fewer grid points per wavelength to obtain any desired accuracy. It successfully solves the frequency dispersion problem which results from a limited difference operator in reverse-time migration. In the numerical computation we apply the phase shift in the frequency domain, change the velocity and anisotropic parameters (ε, σ, ϕ) in the spatial domain, and transform into the frequency domain again in time steps.

NUMERICAL EXAMPLES

To verify the anisotropic reverse-time migration's effectiveness and accuracy, two numerical models are chosen, including P-wave and SV-wave impulse responses, and an anisotropic depth migration with a variable velocity model. The P- and SV-wave impulse

responses show excellent dipping angle imaging ability compared with the phase-shift wave extrapolation shown in (Zhang, et al., 2001). The variable velocity model is designed to exhibit the accurate imaging ability of anisotropic reverse-time migration in TTI media.

P and SV wave migration impulse response

Figure 5 shows the P-wave impulse response in a tilted TI medium with tilt angles of 0, 30, 60, and 90 degrees. Figure 6 corresponds to the SV-wave impulse response. The vertical velocity of the P-wave is 3500m/s and that of the SV-wave is 1500m/s. The homogenous medium has Thomsen anisotropy parameters $\varepsilon = 0.25$ and $\delta = 0.1$. As an illustration of the advantage of reverse-time migration mentioned above, the migration results have clear energy for dipping angles up to 90 degrees. With tilt angles being changed, the symmetric axis changes accordingly. Considering the anisotropy effect, the wavefronts of P-waves and SV-waves differ from the circular ones of an isotropic medium and are consistent with those shown in Figure 3.

Anisotropic depth migration for variable velocity model

A variable velocity model is shown in Figure 7 that consists of one reflector with three horizontal and three dipping segments. The medium has anisotropic parameters $\varepsilon = 0.2$, $\delta = 0.1$ and the tilt angle is 0. Since the tilt angle is zero, the medium is actually VTI. The vertical velocity of the model is v(x, z) =1500+0.3z +0.1x (m/s). Figure 8 shows a synthetic zero offset section for this model. It was generated by an SU (Seismic Unix software available from Center for Wave Phenomena, Colorado School of Mines) anisotropic modeling code that treats transversely isotropic media. Figure 9 is the isotropic migration result obtained from isotropic reverse-time migration method of the 6^{th} order accuracy. Figure 10 shows migration of the anisotropic data in Figure 8 using anisotropic reverse-time migration for TTI media. The correct medium parameters and velocity value are used in the anisotropic RTM. We find that the migration result is an excellent match with the exact model interface. Clearly the image in Figure 10 is superior to that in Figure 9. The image from the isotropic migration (Figure 9) not only is undermigrated but also is placed at a shallow depth. Thus anisotropic RTM gives a substantially better image than the corresponding isotropic RTM. However, the overall runtime of anisotropic RTM is approximately five-times as long as the isotropic case.

PHYSICAL MODEL EXAMPLES

Two scaled physical models, an isotropic reef with a TTI overburden and a TTI thrust sheet in an isotropic background, were constructed by the University of Calgary Foothills Research Project (FRP). These models were used to investigate the magnitudes of imaging error incurred by the use of isotropic processing code when there is seismic velocity anisotropy present in the dipping overburden. The transducer dimensions of the modeling equipment prevented the acquisition of true zero offset; however, we can assume that if the near-offset is close enough to zero, it will be consider zero-offset. Migrations of the collected seismic data exhibit the accurate image positioning of reverse-time anisotropic migration while isotropic migration gives considerable errors in physical position and energy focus.

Depth migration for isotropic reef with a TTI overburden

Seismic data from an anisotropic physical model described by Isaac and Lawton (1999) were used to test the migration algorithm. The cross-section of this model is shown in Figure 11; it includes a TTI overburden layer, 1500m thick, with the axis of symmetry dipping at 45^0. The layer has parameters Vp_0 = 2950m/s, $\varepsilon = 0.241$, and $\delta = 0.100$. An isotropic layer that contains a simulated reef edge with Vp_0 = 2740m/s underlies this anisotropic overburden. Figure 12 shows a zero-offset seismic section with the surface wave muted. To make the first interface of the model migrate to the correct position in the isotropic migration, we consider that the dipping angle is 45^0 and adopt V_{45} for the upper layer. Migration of the zero-offset section by isotropic reverse-time migration yields an image of the reef edge which is displaced by about 350m to the left of its true position (Figure 13). Migration by anisotropic reverse-time migration correctly positions the edge of the reef, as shown in Figure 14. In this case, the input to the migration consisted of a grid containing values of V_{p0}, ε, δ, and tilt of the symmetry axis at each node. Although there are some artifacts caused by interface reflections, these do not affect the basement. The reef is imaged to its true position.

Migration for TTI thrust sheet in an isotropic background

The second physical model is that of a flat reflector overlain by a TI thrust sheet embedded in an isotropic background. The model is shown in Figure 15. The thrust sheet is composed of four blocks in the model; each with a unique axis of symmetry. They have parameters of V_{p0} = 2925m/s, $\varepsilon = 0.224$ and $\delta = 0.100$. The isotropic background has a flat basement with V_{p0} = 2740m/s. The zero-offset seismic section is given in Figure 16. Figures 17 and 18 correspond to isotropic and anisotropic reverse-time migration results. The blue lines in the two figures denote the true location of the thrust sheet interfaces.

With the velocity V_{p0} = 2925m/s for the thrust sheet, the isotropic reverse-time migration result (Figure 17) produces a partial flat basement, whereas the basement beneath thrust sheets exhibits substantial pull up and the energy cannot be focused. The interface between the block with 60 degrees tilted angle and the block with 51 degrees tilted angle is incorrectly positioned since the black solid line does not match with the migration event.

Migration by anisotropic reverse-time migration (Figure 18) leads to more accurate positioning of the reflectors and has nearly flattened the basement reflection, although the reflection event is not continuous. The interfering energy pattern at the base reflector between 2000m and 3300m is believed to indicate a shadow zone caused by the high-velocity thrust sheet overlying slower material. The shadow zone is a result of the zero-offset geometry of the recording. In fact, migration of the prestack data by source-gather migration will fill in the shadow zone due to the multiplicity of ray paths afforded by the prestack geometry (Kumar et al., 2004).

CONCLUSIONS

From the above analysis, it is obvious that anisotropy has a large influence on the accuracy of migrated images. Use of a migration algorithm that takes anisotropy into account, with correct velocity information, can substantially improve images when

anisotropy is present. In this paper, to implement the reverse-time migration in tilted TI media, we first obtained an appropriate P-wave equation to use in place of the isotropic acoustic wave equation employed in isotropic reverse-time migration. With Thomson's weak anisotropy assumption, the wave equation for weakly anisotropic P-waves and SV-waves in tilted transversely isotropic media is derived. Furthermore, the accuracy of the P-wave equation and the SV-wave equation is analyzed and compared with other acoustic wave equations for TTI media. The pseudo-spectral method is easily used to solve these equations, implementing reverse-time migration. According to the migration results from numerical and physical-model seismic data, anisotropic reverse-time migration yields high accuracy for TTI media. The method is encouraging and promising. The computation is still expensive when compared with Kirchhoff migration, and even isotropic reverse-time migration. The computational cost of anisotropic RTM is nearly five times as large as that of isotropic RTM. The reason for this can be seen from an examination of the details of Equation (13). However, with the rapid development of computer hardware, computational cost is no longer the handicap that it has been historically.

ACKNOWLEDGEMENTS

We express our thanks to Dr. Helen Isaac who prepared the model data and to Dr. Chuck Ursenbach for reviewing the manuscript. X. D. also thanks CREWES for financial support and the SEG and CSEG for scholarships. We appreciate Center for Wave Phenomena (CWP), Colorado School of Mines for use of free Seismic Unix software.

REFERENCES

Alkhalifah, T., 1995, Gaussian beam depth migration for anisotropic media: Geophysics, **60**, 1474-1484.

Alkhalifah, T., 2000, An acoustic wave equation for anisotropic media: Geophysics, **65**, 1239-1250.

Baumstein, A. and Anderson, J., 2003, Wavefield extrapolation in laterally varying VTI media, 73rd Ann. Internat. Mtg.: Soc. of Expl. Geophys., 945-948.

Daley, P. F, and Lines, L. R., 2004, Linearized quantities in transversely isotropic media, Canadian Journal of Earth Sciences, **41**, 349-354.

Ferguson, R. and Margrave G. F., 1999, Depth migration in TI media by non-stationary phase shift. 68th SEG meeting, New Orleans, U.S.A., Expanded Abstracts, 1831-1834.

Fornberg, B. 1987, The pseudospectral method - Comparisons with finite differences for the elastic wave equation: Geophysics, **52**, 483-501.

Grechka, V., Zhang, L. and Rector, J., 2004, Shear waves in acoustic anisotropic media: Geophysics, 69, 576-582.

Isaac, J. H., and Lawton, D. C., 1999, Image mispositioning due to dipping TI media: A physical seismic study: Geophysics, **64**, 1230-1238.

Klie, H., and Toro, W., 2001, A new acoustic wave equation for modeling in anisotropic media: 71st 72Annual International meeting, SEG, Expanded Abstracts, 1171–1174.

Kumar, D., Sen M. K., and Ferguson, R. J., 2004, Traveltime calculation and prestack depth migration in tilted transversely isotropic media: Geophysics, **69**, 37-44.

McMechan, G. A., 1983, Migration by extrapolation of time-dependent boundary values: Geophys. Prosp., **31**, 413-420.

Thomsen, L., 1986, Weak elastic anisotropy: Geophysics, **51**, 1954–1966.

Tsvankin, I., 1996, P-wave signatures and notation for transversely isotropic media: An overview: Geophysics, **61**, 467-483.

Vestrum, R. W., Lawton, D. C. and Schmid, R., 1999, Imaging structures below dipping TI media: Geophysics, **64**, 1239-1246.

Wu, W., Lines, L. R., and Lu, H., 1996, Analysis of higher-order, finite-difference schemes in 3-D reverse-time migration: Geophysics, **61**, 845-856.

Yoon, K., Shin, C, Suh, S., Lines, L. R., and Hong S., 2003, 3D reverse-time migration using acoustic wave equation: An experience with the SEG/EAGE data set: The Leading Edge, **22**, 38-41.

Zhang, J., Verschuur, D. J. and Wapenaar, C. P. A., 2001, Depth migration of shot records in heterogeneous, tranversely isotropic media using optimum explicit operators: Geophys. Prosp., **49**, 287-299.

Zhang, L., Rector, J. W., and Hoversten, G. M., 2003, An acoustic wave equation for modeling in tilted TI media: 73rd Annual International Meeting, SEG, Expanded Abstracts, 153–156.

FIGURES

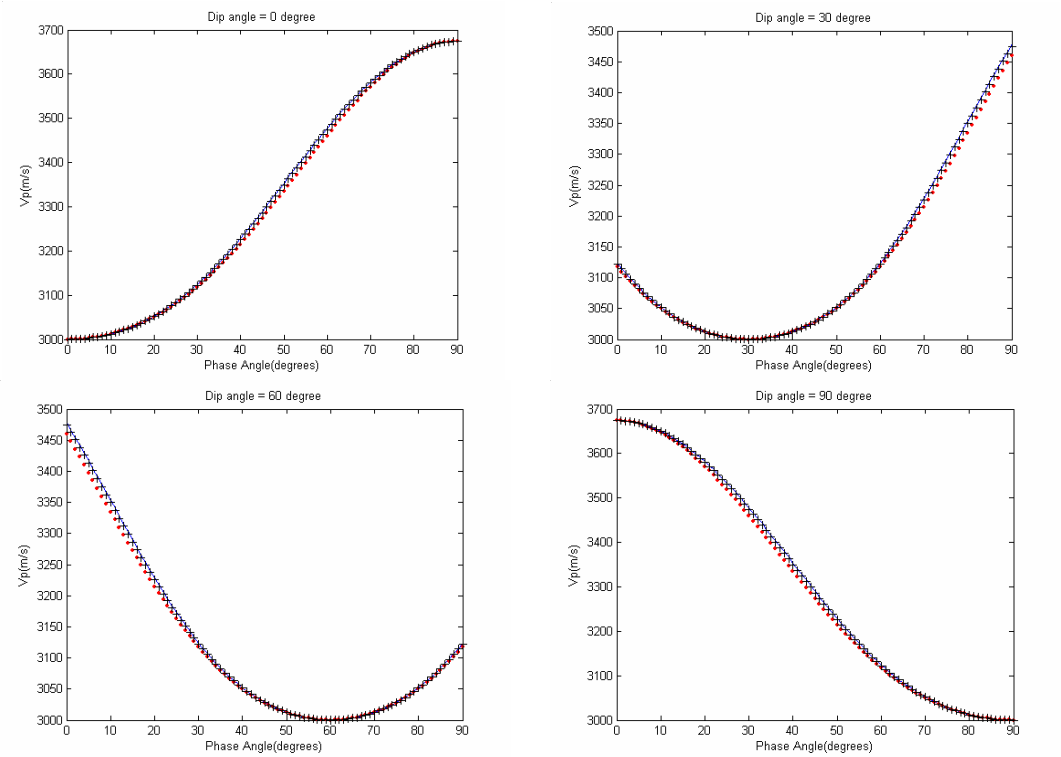

FIG. 1. P-wave phase velocity. The black line corresponds to the Alkhalifah formula, the red one to the weak anisotropy formula, and the solid one to the exact formula.

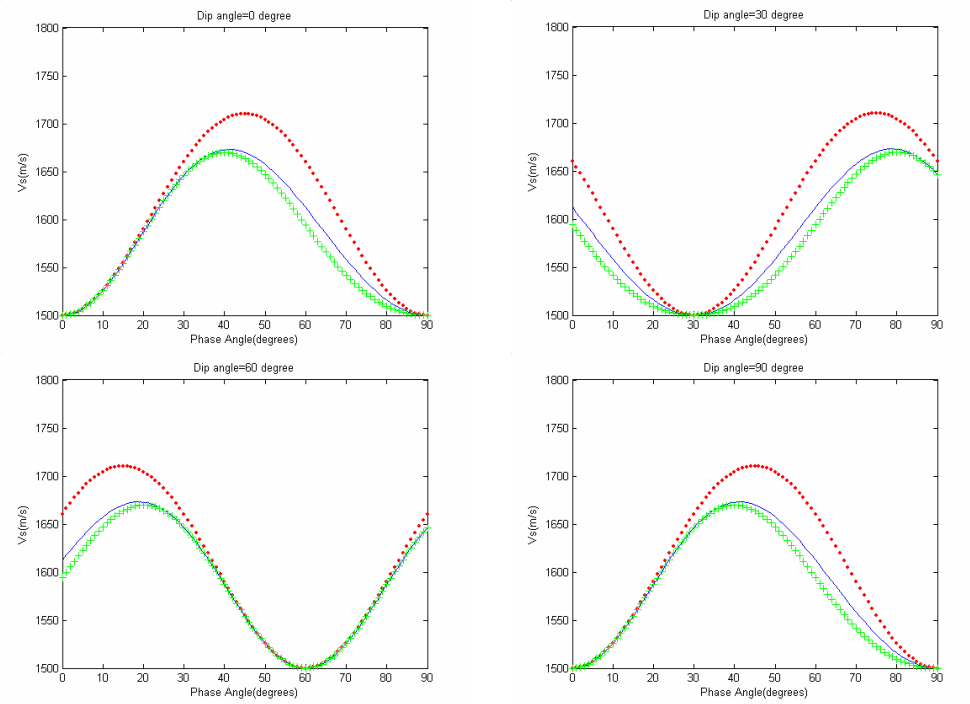

FIG. 2. SV-wave phase velocity. The red curves correspond to the weak anisotropy formula with linear approximation, the green curves denote weak anisotropy with quadratic approximation and the blue curves the exact formula.

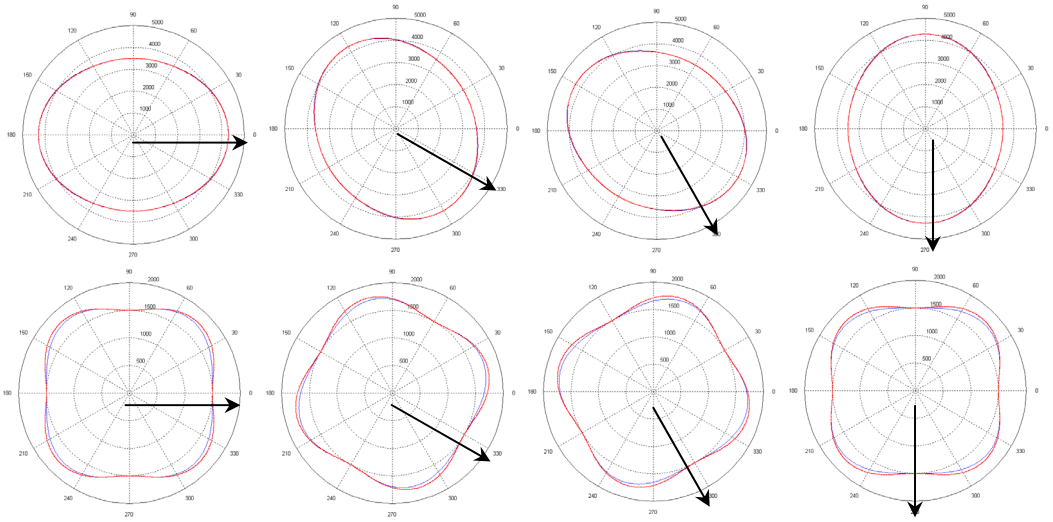

FIG. 3. P and SV-wave phase velocity. The red curves correspond to the weak anisotropy formula and the solid line to the exact formula. The upper four graphs correspond to the P-wave and the bottom four to the SV-wave. The graphs from left to right denote the results with tilted angle 0^0, 30^0, 60^0, and 90^0.

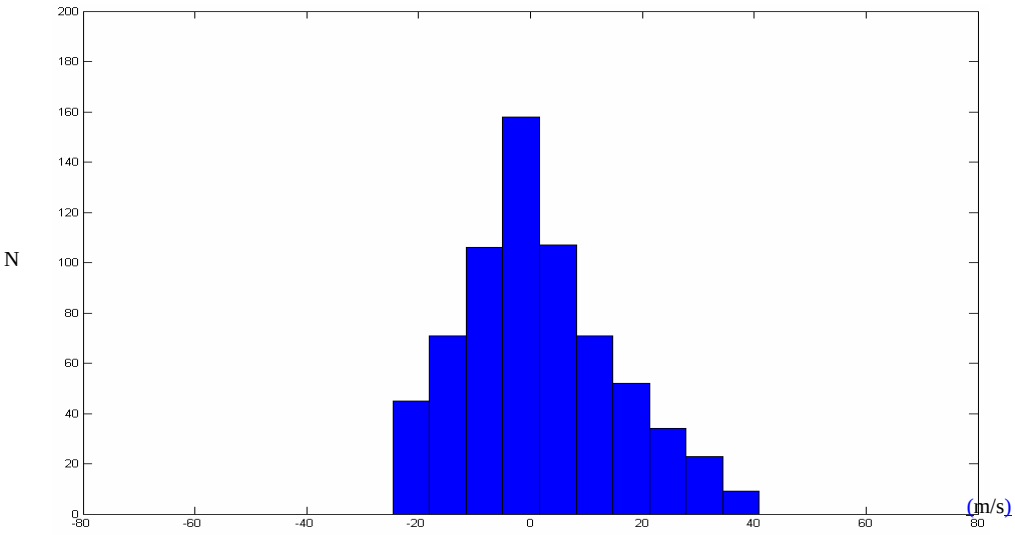

FIG. 4. Absolute maximum difference distribution between simplified P-wave velocity formula and exact formula.

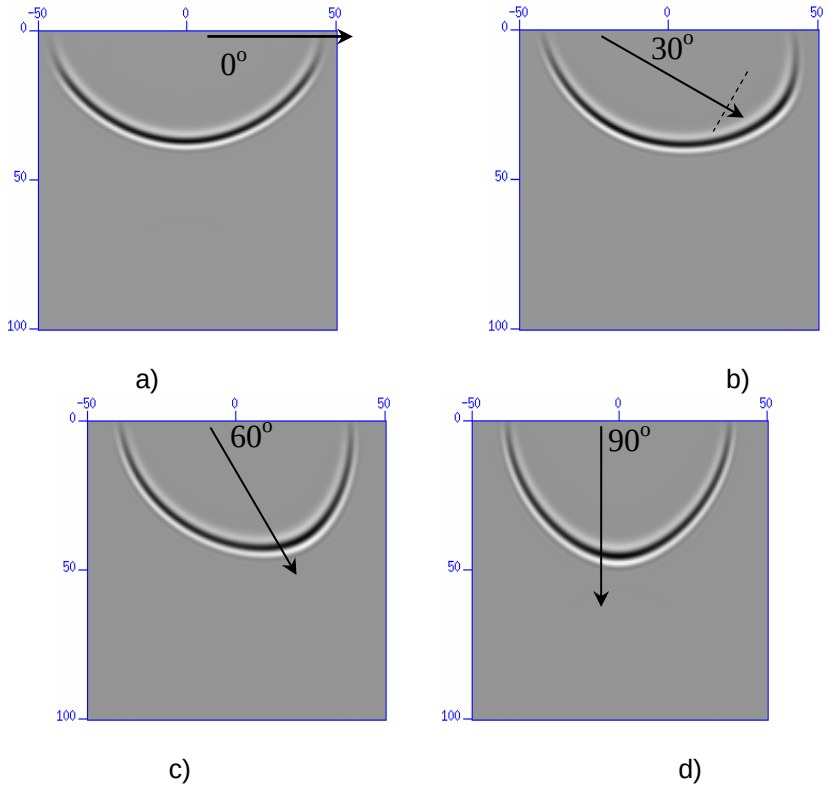

FIG. 5. P- wave impulse response. (a), (b),(c) and (d) correspond to the result of a tilt angle of 0, 30, 60, and 90 degrees as indicated by the arrows.

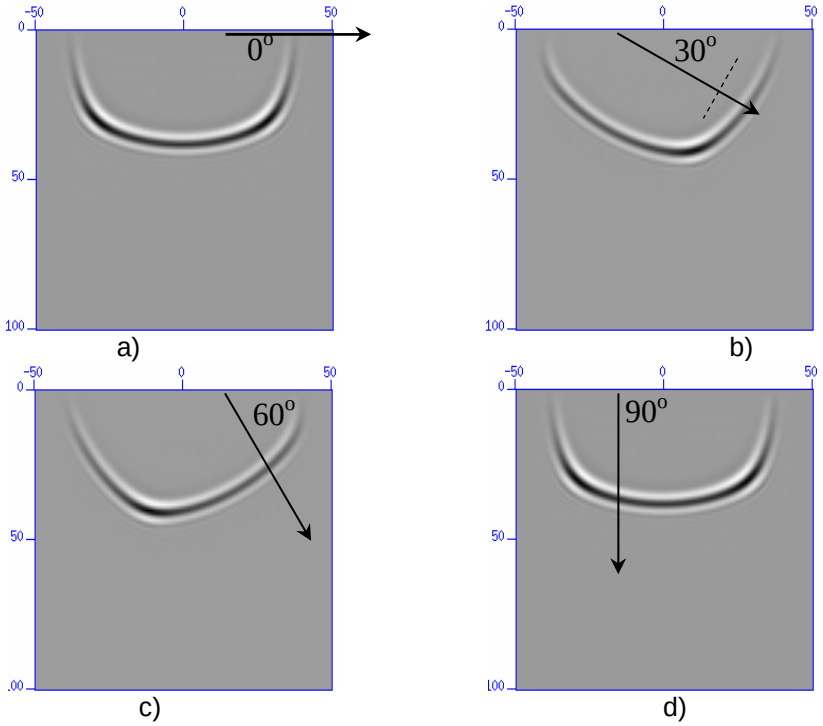

FIG. 6. SV-wave impulse response. (a), (b), (c) and (d) correspond to the result of a tilt angle of 0, 30, 60, and 90 degrees.

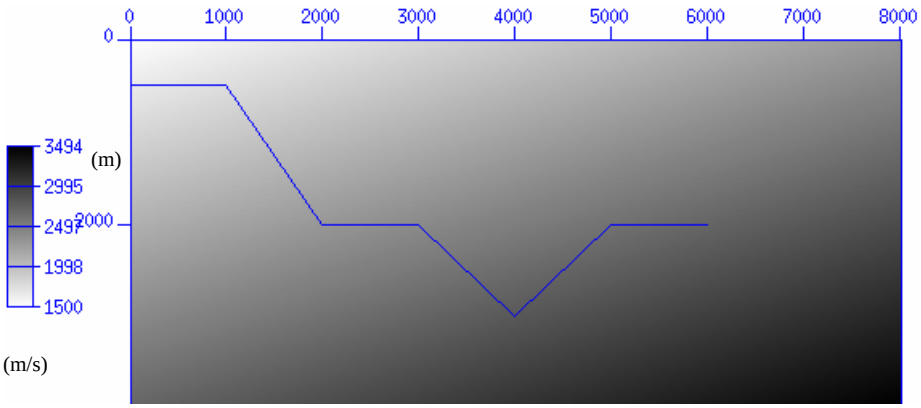

FIG. 7. Variable velocity model.

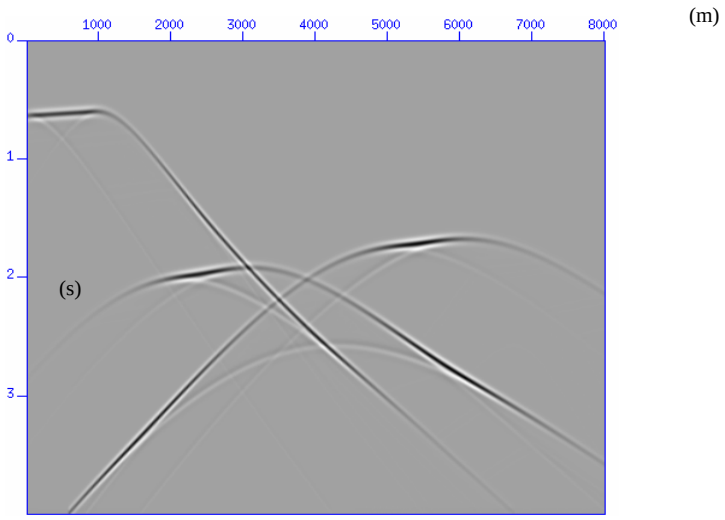

FIG. 8. Synthetic zero-offset seismogram obtained using an SU code from Center for Wave Phenomena (CWP) for the structural model of Figure 7 for TI media.

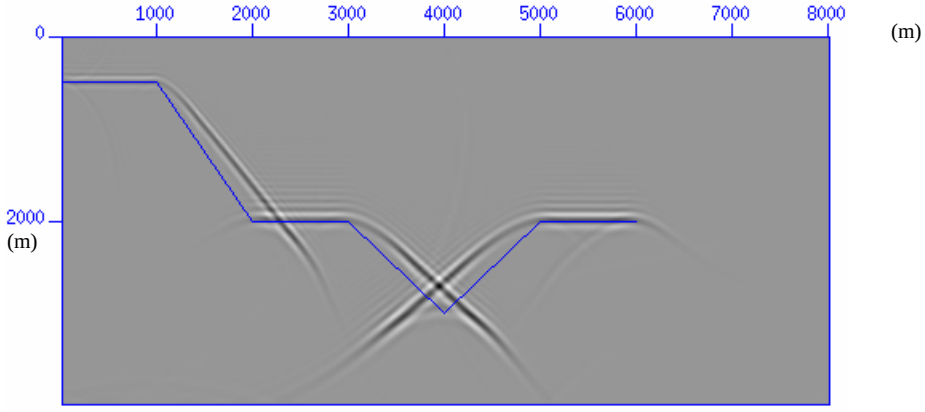

FIG. 9. Migration result by the isotropic reverse-time migration method.

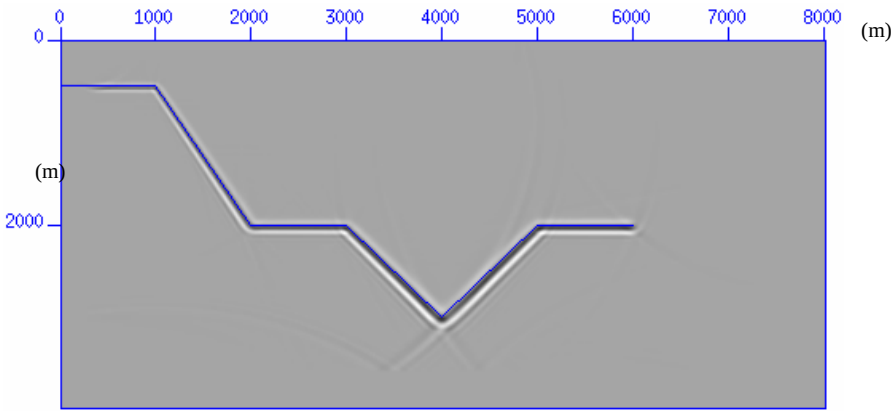

FIG. 10. Migration result from the anisotropic reverse-time migration method.

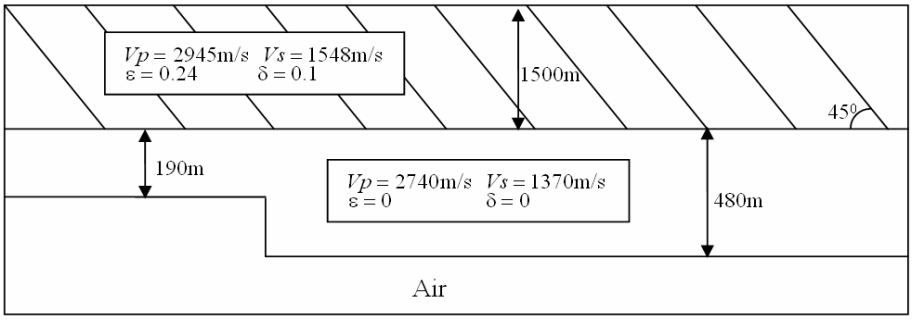

FIG. 11. Isotropic reef with a TTI overburden.

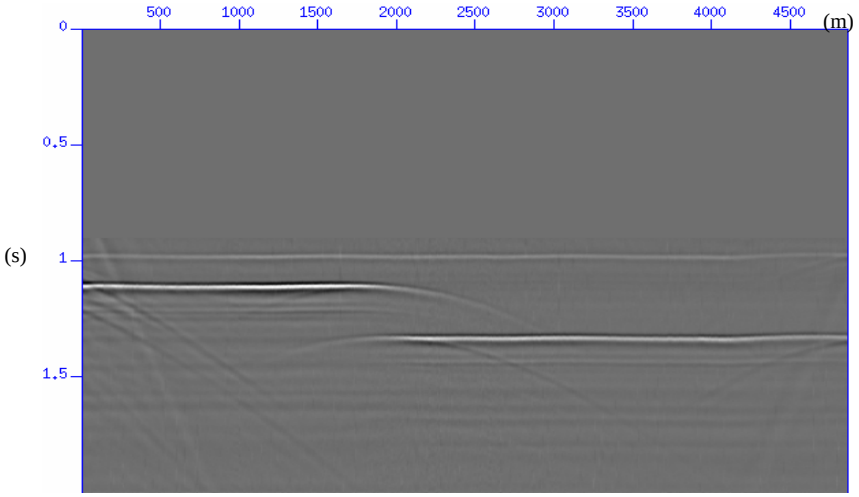

FIG. 12. Zero-offset seismic section of reef model.

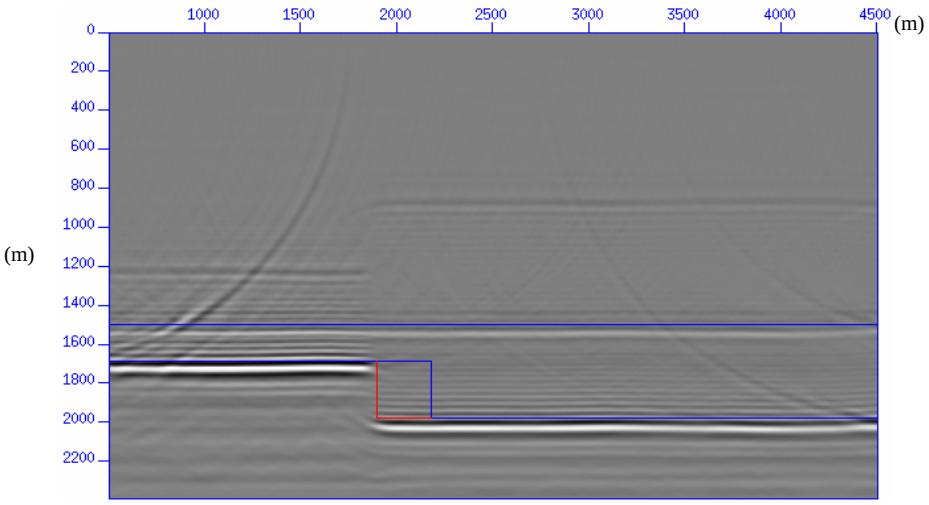

FIG. 13. Isotropic reverse-time migration result of the 6th order accuracy for reef model.

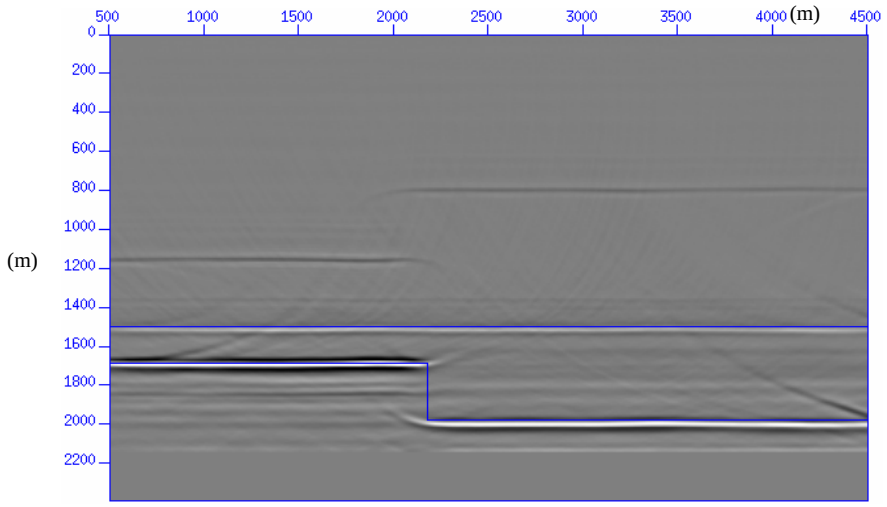

FIG. 14. Anisotropic migration result of reef model.

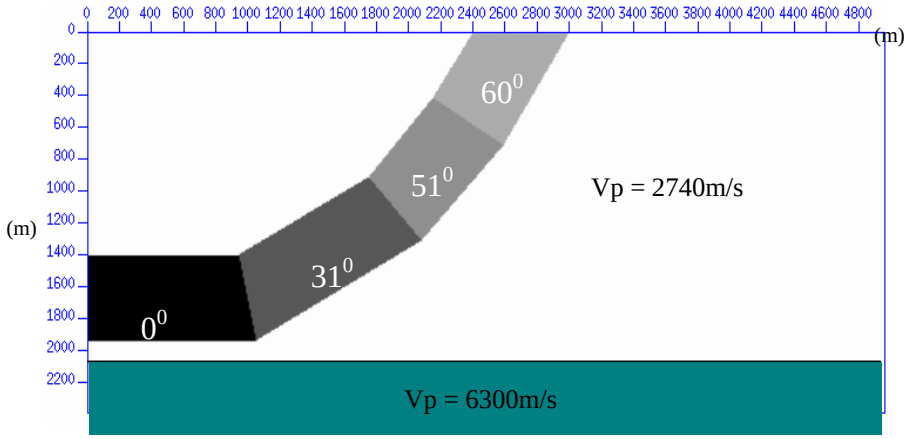

FIG. 15. TTI thrust model.

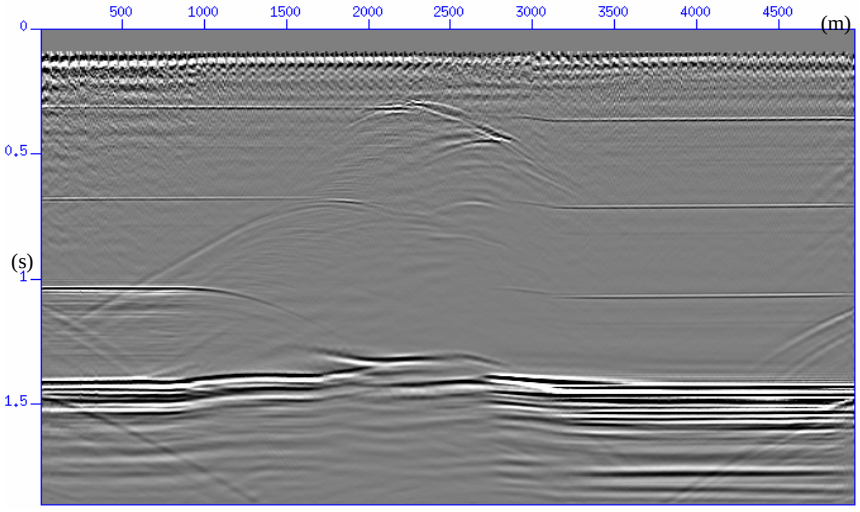

FIG. 16. Zero-offset seismic section of TTI thrust model.

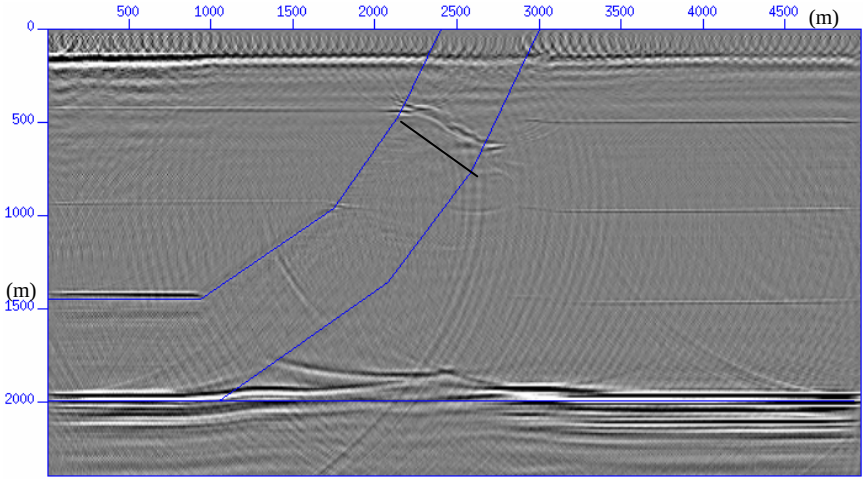

FIG. 17. Isotropic reverse-time migration result of TTI thrust model.

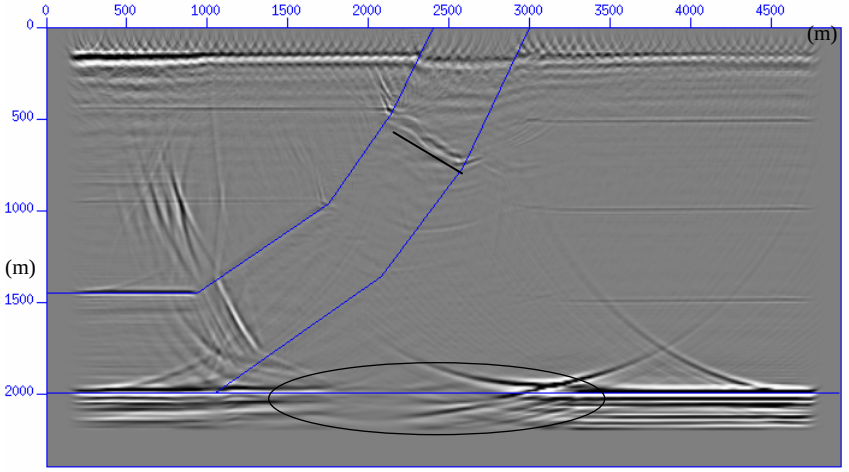

FIG. 18. Anisotropic reverse-time migration result of TTI thrust model.